Journal of Thermal Analysis and Calorimetry (2020) 141:807–817
https://doi.org/10.1007/s10973-019-09044-4

Thermochemical and kinetic study of the attack of fluorapatite by sulfuric acid solution at different temperatures

Hadir Aouadi-Selmi[1] · Kaïs Antar[1] · Ismail Khattech[1]

Received: 30 July 2018 / Accepted: 8 November 2019 / Published online: 21 November 2019

Abstract
The thermochemical and kinetics study of the attack of a synthetic fluorapatite (Fap) by a 10 mass% H_2SO_4 sulfuric acid solution was performed first at 25 °C using C-80 SETARAM microcalorimeter with reversal cells. The results are repetitive only for few amounts of Fap and the global enthalpy of the attack equals -401.4 ± 9.7 kJ mol^{-1}. The recorded curves and thermogenesis show one peak corresponding to the formation of anhydrous calcium sulfate (AH). The Avrami model has been used in order to determine the Avrami constants (k and n). The deconvoluted curves agree with a homogeneous kinetic scheme based on two successive reactions of order 1 with respect to calcium involving dissolution and precipitation phenomena. The precipitation enthalpy of AH deduced from iteration is close to the one determined experimentally and the sum of the reaction enthalpies does not differ from the global enthalpy determined by integrating the rough signal by more than 2.8%. Increasing temperature led to an increase in the attack rate, and kinetic results agree with the shrinking core model with a mixture of both diffusion through an ash layer and chemical reactions control. The two resulting apparent activation energies are 34.4 and 41.0 kJ mol^{-1}, which are in the range determined by the isoconversional model [16.7–48.8 kJ mol^{-1}].

Keywords Fluorapatite · Microcalorimetry · Kinetics · Dissolution · Precipitation enthalpy

Introduction

Phosphate fertilizers are produced from phosphate ore. The attack of the latter by a solution of sulfuric acid and/or phosphoric acid is the basic process for the production of phosphoric acid and inorganic fertilizers such as superphosphates.

The study of chemical behavior, in particular dissolution kinetics and mechanisms under various conditions of natural apatite in industrial processes, is of fundamental interest. A number of investigations devoted to natural apatite dissolution kinetics and mechanisms in water, buffers, and acidic media have already been reported [1–5].

Sevim et al. dissolved Turkish mineral phosphates in sulfuric acid solution and found that the rate of dissolution increases with increasing temperature and acid concentration and decreases with increasing particle size and the solid–liquid ratio [6]. Recently, Balsam et al. [7] have studied the thermodynamics and kinetics of the dissolution of natural phosphate rocks with two different concentrations of P_2O_5 and have demonstrated that the granulometry distribution plays an important role in this attack.

Several studies dealt with the study of the acid attack of synthetic apatites by calorimetry. For example, Jemal et al. [8] have determined the formation enthalpies of fluorapatite, hydroxyapatite and chloroapatite by dissolution in nitric acid (9%).

The attack of a synthetic fluorapatite (Fap) with phosphoric acid was carried out by Brahim et al. [9]; they showed that the Fap digestion reaction at 25 °C with a phosphoric acid solution containing 10, 18 or 30% mass% P_2O_5 occurred in two steps. The first corresponds to the dissolution of the solid in phosphoric acid and the second to the formation of the $Ca(H_2PO_4)^+$ complex. On the other hand, Antar et al. [10] studied the attack, at 25 °C, of synthetic fluorapatite by mixtures of sulfuric and phosphoric acid and showed the existence of two stages. The first one has been attributed to the dissolution of the solid, and the second one to precipitation of gypsum.

✉ Kaïs Antar
kais.antar@fst.utm.tn

[1] LR15ES01, Materials, Cristallochemistry and Applied Thermodynamics Laboratory, Chemistry Department, Faculty of Science of Tunis, University of Tunis El Manar, 2092 Tunis El Manar, Tunisia

To better understand the kinetic aspect of the sulfuric attack of natural apatites, synthetic Fap could provide instructive information.

In the wet process of the production of phosphoric acid (H_3PO_4), attack by sulfuric acid is one of the important steps. As far as we are aware, there are no reports on the thermochemical and kinetic study of the latter by microcalorimetry.

The aim of this work is to model the attack reaction of synthetic fluorapatite by a 10 mass% H_2SO_4 sulfuric acid solution at 25 °C and then in the temperature range of 30–45 °C using the microcalorimetry technique.

Experimental

Fluorapatite was synthesized using the double decomposition method recommended by Heughebaert [11] and consists in adding, dropwise, during 3 h, an ammonium phosphate ($(NH_4)_2HPO_4$: FLUKA, purity > 99.9%.) solution and ammonium fluoride (NH_4F, ACROS, purity > 99.9%.) solution into a boiling solution of calcium nitrate ($CaNO_3{\cdot}4H_2O$ ACROS, purity > 99.9%.). The pH was adjusted between 8 and 9 by adding ammonia solution (28 mass%). After filtration, the solid was washed and dried overnight at 70 °C and then heated at 800 °C for 24 h under Argon flow. It was then characterized by X-ray diffraction and infrared spectroscopy.

X-ray diffraction was carried out by a D8-ADVENCE Brucker diffractometer using copper radiations ($K\alpha_1 = 1.5406$ Å; $K\alpha_2 = 1.5445$ Å). And infrared spectrum was recorded using a Perkin-Elmer 7700 FTIR spectrometer between 4000 and 400 cm^{-1} in KBr pellet.

For the thermochemical and kinetic study, a C-80 SETARAM microcalorimeter operating in isothermal mode was used in its reversal cells version. After a stabilization time of one night at the chosen temperature, experiments were carried by dissolving *m* (mg) of Fap in 4.5 mL of sulfuric acid solution (10 mass% H_2SO_4). The recorded signals were processed according to the procedure described by Brahim et al. [9] in order to get the time constants of the devise allowed to calculate the deconvoluted curves for each dissolved Fap mass. Because of the rapidity of the phenomenon, the kinetic study has been undertaken only considering these curves.

Results and discussion

X-ray pattern of the synthetized Fap is given in Fig. 1. The latter confirms that the solid was a pure Fap which crystallizes in the hexagonal system $P6_3/m$. The structure was refined by a cell parameter refinement program "ERACEL." Table 1 gives crystallographic parameters of Fap [12]. Figure 2 gives the IR spectrum of the synthetic Fap, which shows the characteristic absorption bands of Fap and does not reveal any impurities such as HPO_4^{2-} (1180–1200, 875 cm^{-1}), CaO (3640 cm^{-1}), $P_2O_7^{4-}$ (1200–1250 cm^{-1}) or OH^- ions. The latter are characterized by a sharp peak at 3560 cm^{-1}.

Attack of the fluorapatite at 25 °C

Thermochemical study

For Fap masses lower than 40 mg, the sulfuric acid attack leads to repetitive experiments and both rough and deconvoluted curves show one peak. Figure 3 gives examples of these curves.

Figure 4 shows the variation of the thermal energy determined by integrating the raw signal, as a function of the

Table 1 Crystallographic parameters of the fluorapatite

	a/Å	*c*/Å
Present work	9.372 ± 0.003	6.884 ± 0.002
Literature [11]	9.373 ± 0.005	6.882 ± 0.005

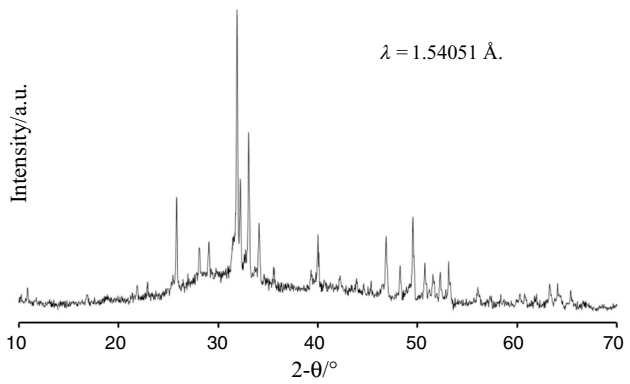

Fig. 1 X-ray diffraction of fluorapatite

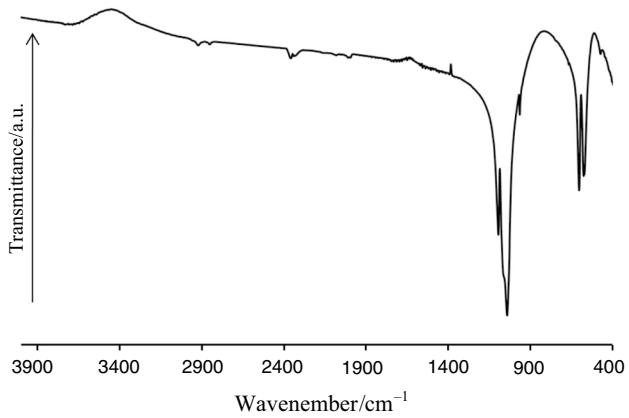

Fig. 2 Infrared spectra of the Ca-Fap

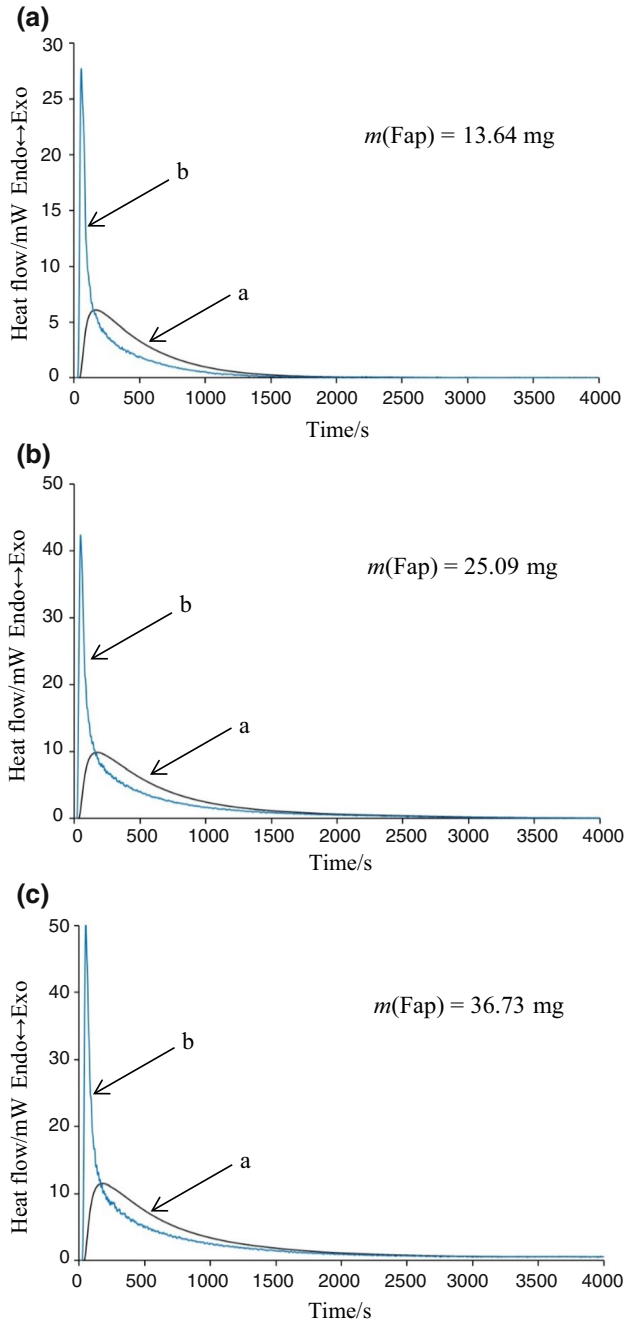

Fig. 3 Raw (**a**) and deconvoluted (**b**) curves corresponding to the attack of different masses of Fap

dissolved Fap masses. The slope of the curve enables to calculate a molar enthalpy as $\Delta H = -401.4 \pm 9.7$ kJ mol^{-1}. The errors were determined using the mathematical procedure developed by Pattengill and Sands [13, 14].

The solid isolated at the end of the sulfuric attack is the anhydrous calcium sulfate ($CaSO_4$) which is identified by X-ray diffraction Fig. 5.

The plot of the molar enthalpies as a function of dissolved Fap masses (not reported) leads to a horizontal line

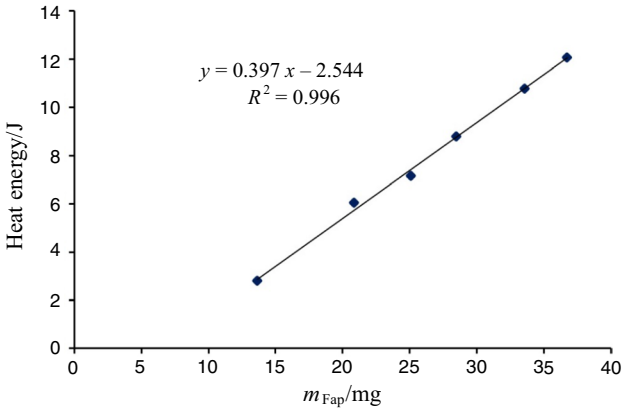

Fig. 4 Heat energy versus fluorapatite masses at 25 °C

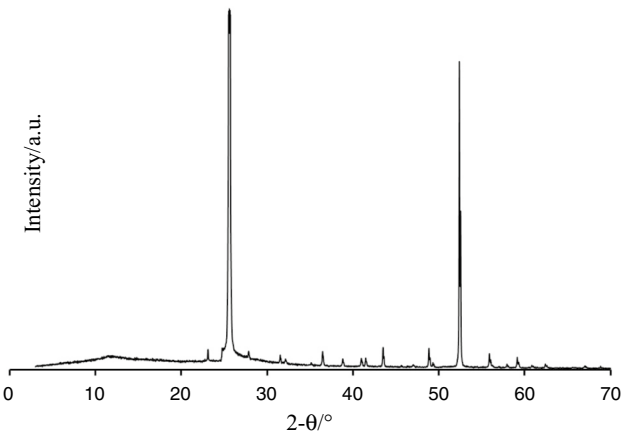

Fig. 5 X-ray diffraction of the solid isolated after the attack of Fap by sulfuric acid solution (10 mass% H_2SO_4) at 25 °C

suggesting that the former quantity is independent on the dissolved mass.

Kinetic treatment

Avrami model This model links the reactant transformed fraction x to time t by the following equation:

$$-\ln(1-x) = kt^n$$

with n and k being the Avrami constants. Avrami parameters for successive steps in the global process can be deduced from the drawing of $\ln(-\ln(1-x))$ versus $\ln(t)$.

At the origin, this model has been formulated for crystallization of solids from pure liquid [15] and the slope change in the curve has been attributed to the appearance of a new phenomenon during a phase change [16–18]. This model has been extended to chemical process as dissolution and precipitation. Kabai [19] applied this model for the interpretation

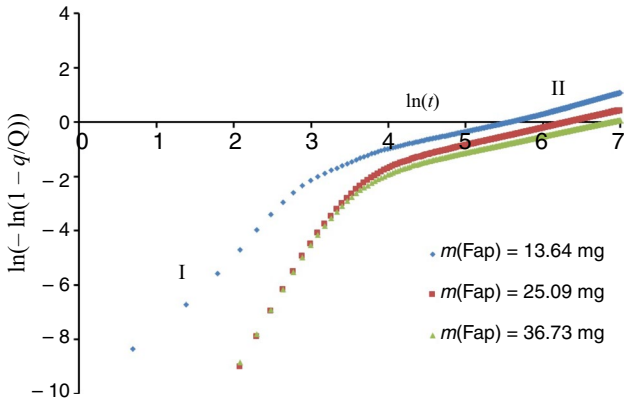

Fig. 6 Plot of $\ln(-\ln(1-x))$ versus $\ln(t)$ for various masses of fluorapatite

of dissolution of more than 50 metals and oxides. The same model has been used to interpret the dissolution and precipitation of several products [6, 10, 20–22]. In the present case, fraction x equals the ratio of the heat q released at time t over the overall heat Q_t. These quantities were determined by integrating their corresponding area under the recorded peak.

Figure 6 gives the Avrami curves for various amounts of attacked Fap. The curves exhibit two domains I and II suggesting a two-step dissolution process. The duration of the first step is about 33 s ($\ln 33 \approx 3.5$), whereas the second one occurs during a much longer time (about 1800 s). However, the first domain is too short to be kinetically explored; consequently, as with the work of Zendah et al. [23], the kinetic study has been conducted only on the second domain. Table 2 gathers the values of k and n parameters corresponding to this domain. The Avrami parameter n varies from 0.56 to 0.73. The first value (0.56) was found in a previous work [10], and the second one (0.73) is close to the one obtained by Sevim et al. [6] (0.7) during the attack of natural phosphate by sulfuric acid. Values of the constant k are in the range of 0.017 and 0.021. The literature does not suggest any interpretation for different values of this factor, while some phenomena have been attributed to particular values of n. In our case, n lies between 0.5 and 0.73. The Avrami exponent n is characteristic of the phase growth mode and geometry [24]. Papon et al. [24] and Hubert [25] have attributed $n=0.5$ to a diffusion-controlled growth with plane geometry and rapidly exhausted nucleation. Kuga and Sêsták [26] have assigned the latter value of n to one-dimensional growth of nuclei controlled by diffusion. Also, Roland Fotsing [27] has attributed $n=0.5$ to a one-dimensional growth from preexisting nuclei and has described this stage as: no more new nuclei can be formed at grain boundaries due to impingement and only the already nuclei may grow. For $n<1$, Brahmia [28] has described one-dimensional growth for heterogenous germination. According to Rao and Rao [29], the value 0.5 of the Avrami exponent has been attributed to the "thickening of plates after their edges have impinged".

Homogeneous kinetic scheme To reveal the attack mechanism corresponding to the deconvoluted curve, a number of hypothesis have suggested. Then, the iteration was carried out in order to obtain the best coincidence between the calculated curves and the thermogenesis. The calculation shows that the process in two successive step leads to a better coincidence. This mechanism is represented by the following scheme:

$$A(\text{Fap}) + \text{sol} \xrightarrow{k_1} B, \text{ with rate constant } k_1 \quad \text{(I)}$$

$$B \xrightarrow{k_2} C, \text{ rate constant } k_2 \quad \text{(II)}$$

where k_1 and k_2 are the respective kinetic constants.

Considering that these reactions are of order 1 with regard to A and B, respectively, the equation rates are in the form:

$$r_1 = k_1 C(A) \quad (1)$$

$$r_2 = k_2 C(B) \quad (2)$$

where $C(A)$ and $C(B)$ are the molar concentrations of A and B, respectively.

If the first reaction is not perturbed by the second reaction, the concentration of reagent A is given by the relationship below:

$$C(A) = C_o(A) \exp\left(-k_1 t\right) \quad (3)$$

with $C_o(A)$ is the initial concentration of A.

Moreover, the component B formed by the first reaction is consumed by the second one and, therefore, its global appearance rate can be expressed as follows:

$$r(B) = r_1 - r_2 \quad (4)$$

or

$$-\frac{dC(B)}{dt} = k_2 C(B) - k_1 C(A) \quad (5)$$

The integration of Eq. (5) leads to the following expression for the concentration of B:

$$C(B) = C_0 \frac{k_1}{k_1 - k_2}\left(\exp\left(-k_2 t\right) - \exp\left(-k_1 t\right)\right) \quad (6)$$

Conservation of the mass implies that at any time the sum of the concentrations of the species A, B and C is equal to the initial concentration of reagent A and therefore:

Table 2 Avrami parameters (k and n) corresponding to domains II of Fig. 6, for various Fap masses

Fap masses/mg	k	n
13.64	0.017	0.73
25.09	0.021	0.60
36.73	0.019	0.56

$$C(A) + C(B) + C(C) = Co(A)$$

and

$$C(C) = C_0\left[1 - \frac{k_2 \exp\left(-k_1 t\right) - k_1 \exp\left(-k_2 t\right)}{k_2 - k_1}\right] \quad (7)$$

If q_1 designates the quantity of heat released at time t by transforming an amount of material of A into B, then:

$$q_1 = \left[C_o(A) - C(A)\right] V \Delta_1 H \quad (8)$$

with V the medium volume of the reactional; $\Delta_1 H$ the molar enthalpy of reaction (I).

The quantity of heat q_2 resulting from the transformation of an amount of B into C is expressed as

$$q_2 = C(C) V \Delta_2 H \quad (9)$$

with $\Delta_2 H$ the molar enthalpy of reaction (II).

The total heat (q) measured during the experiment is expressed by the following equation:

$$q = q_1 + q_2$$

The heat flow can be deduced as follows:

$$\frac{\mathrm{d}q}{\mathrm{d}t} = \frac{m_\mathrm{A}}{M_\mathrm{A}}\left[\frac{\Delta_2 H k_1 k_2}{k_1 k_2}\left(\exp\left(-k_2 t\right) - \exp\left(-k_1 t\right)\right) + \Delta_2 H k_1 \exp\left(-k_1 t\right)\right] \quad (10)$$

with M_A: the molar mass of Fap (1008.6 g mol^{-1}) and m_A its initially introduced mass.

Iteration of Eq. (10) is undertaken by searching k_1, k_2, $\Delta_1 H$ and $\Delta_2 H$ values to give a better coincidence between the calculated and the deconvoluted curves.

Figure 7 shows an example of an iteration result for two masses of Fap, which reveals a good agreement between the calculated and the thermogenesis curves. Also, an agreement was obtained for the values of the kinetic and thermodynamic parameters for different fluorapatite masses (Table 3).

One can notice slight variations of these parameters. Furthermore, the sum of the average values of $\Delta_1 H$ and $\Delta_2 H$ ($\Delta_1 H + \Delta_2 H$) is -412.93 kJ mol^{-1}. This value does not differ from the enthalpy determined by integrating the rough signal (-401.4 kJ mol^{-1}) by more than 2.8%, confirming the validity of the model.

In this hypothesis, we can propose this mechanism:

The first step of this mechanism can be attributed to the Fap dissolution:

$$\mathrm{Ca_{10}(PO_4)_6F_{2(s)}} + 10\left\{\mathrm{H_2SO_4}\right\}_{\mathrm{sol}} \rightarrow \left\{10\mathrm{Ca^{2+}} + 10\mathrm{SO_4^{2-}} + 6\mathrm{H_3PO_4} + 2\mathrm{HF}\right\}_{\mathrm{sol}} \quad (III)$$

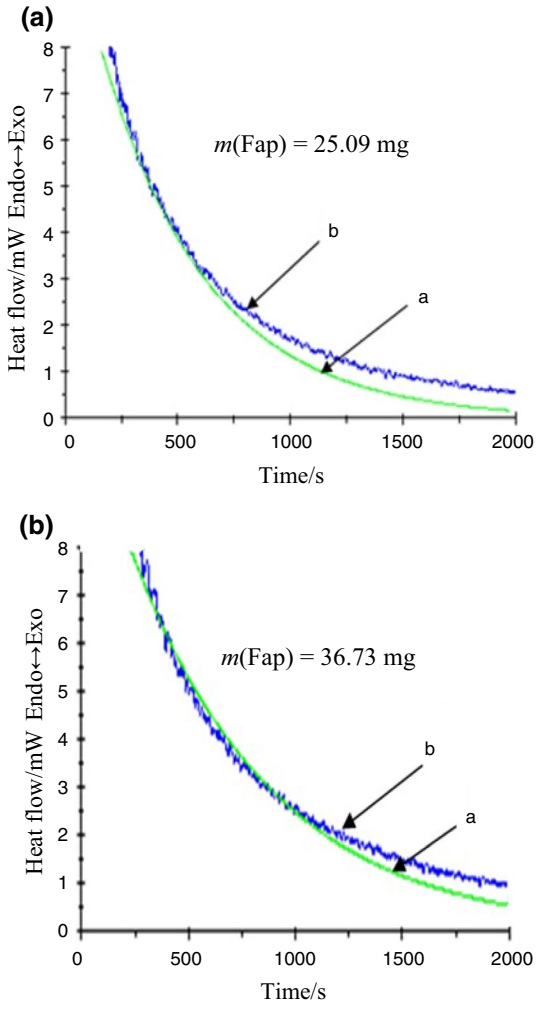

Fig. 7 Iteration curve of Eq. (10) (**a**) and thermogenesis (**b**) one for two masses of Fap

And the second one could correspond to the anhydrous calcium sulfate precipitation. Because of their overlapping, these phenomena do not appear on Avrami curves:

$$\left\{10\mathrm{Ca^{2+}}\right\}_{\mathrm{sol}} + \left\{10\mathrm{SO_4^{2-}}\right\}_{\mathrm{sol}} \rightarrow 10\mathrm{CaSO_{4(s)}} \quad (IV)$$

In this case, the global reaction of the attack of Fap by 10 mass% H_2SO_4 solution would be the following:

$$\mathrm{Ca_{10}(PO_4)_6F_{2(s)}} + 10\{\mathrm{H_2SO_4}\}_{\mathrm{sol}} \rightarrow \left\{6\mathrm{H_3PO_4}\right\}_{\mathrm{sol}} + \{2\mathrm{HF}\}_{\mathrm{sol}} + 10\mathrm{CaSO_{4(s)}} \quad (V)$$

Comparing kinetic constants, in Table 4, for the first step of the two successive step process relative to reaction (I) attributed to the Fap dissolution obtained in the present work and in previous works in the case of the Fap attack by the phosphoric acid solution at 25 °C [9] and by the mixtures of sulfuric and phosphoric acids solutions at 55 °C [30], we can

Table 3 Kinetic and thermodynamic parameters deduced by iteration of Eq. (10) for various masses of Fap

Fap masses/mg	$k_1/s^{-1} \times 10^3$	k_2/mol L^{-1} s^{-1}	$-\Delta_1 H$/kJ mol^{-1}	$-\Delta_2 H$/kJ mol^{-1}
13.64	2.99	1.47	185.1	227.7
25.09	2.11	1.47	190.9	227.4
36.73	2.69	1.46	180.9	226.8

Table 4 Kinetic constants for the first step of the two successive step process relative to reaction (I) attributed to the Fap dissolution

	Current work	Ref. [24]	Ref. [8]
$k_1/s^{-1} \times 10^3$	[2.11; 2.99]	[2.61; 2.71]	[4.14; 6.64]

notice that the Fap dissolution in the sulfuric acid solution is much lower than the phosphoric one [9] at the same temperature (25 °C), however, is much faster when comparing this constant to the one obtained at 55 °C in the case to the mixtures of sulfuric and phosphoric acids solutions attack.

Direct measurement of the precipitation enthalpy of $CaSO_4$

The precipitation enthalpy value of anhydrous calcium sulfate (− 227.3 kJ mol^{-1}) deduced from iteration can be determined experimentally by performing experiments in conditions similar to that corresponding to the attack of Fap. This consists in measuring the energy resulting from the addition of calcium nitrate solution ($Ca(NO_3)_2$), 0.27 M) to a sulfuric acid solution (13.36% H_2SO_4). These concentrations were chosen in order to get a final concentration of Ca^{2+} and SO_4^{2-} in the same order of magnitude as that obtained by dissolving Fap in H_2SO_4 solution (10 mass% H_2SO_4). IR spectroscopy shows that the solid isolated after these experiments was the anhydrous calcium sulfate. Indeed, this solid exhibits absorption bands, Fig. 8, similar to that cited by Mandal and Mandal [31] for anhydrous calcium sulfate.

Various amounts (mg) of calcium nitrate solution were added to 1.5 mL of sulfuric acid solution. The resulting measured energy is represented in Fig. 9a and can be expressed as:

$$\Delta_1 H = 0.008m - 0.523 \quad (11)$$

This quantity corresponds not only to precipitation of anhydrous calcium sulfate but also to dilution of the acid. The latter has been determined by mixing various masses (mg) of pure water with 1.5 mL of the acid solution. The resulting energy is expressed by the following equation, (Fig. 9b):

$$\Delta_2 H = 0.001m + 0.142 \quad (12)$$

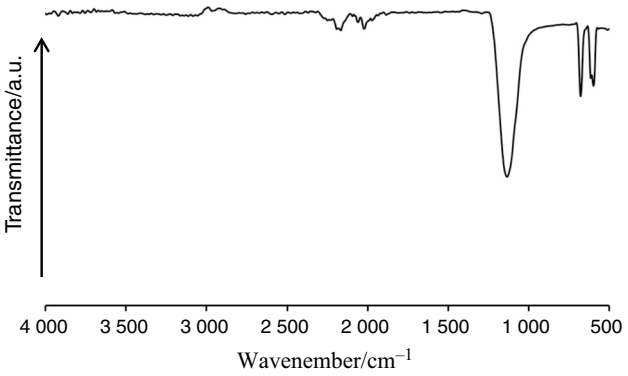

Fig. 8 Infrared spectra of the solid isolated after the experiments of the direct $CaSO_4$ measurement precipitation enthalpy

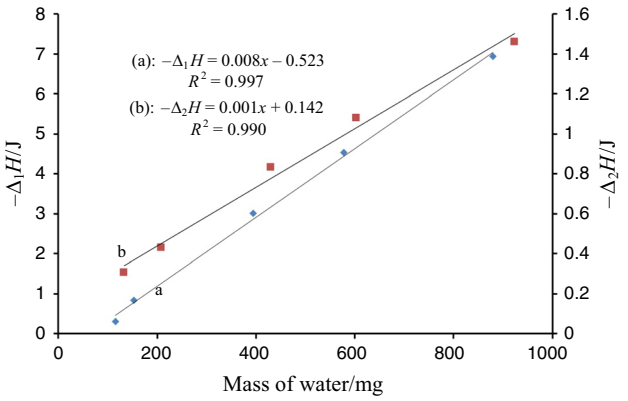

Fig. 9 Measured energy versus the mass of water

The precipitation enthalpy can be deduced from the deference between the heat quantities given by curves *a* and *b* for a given amount of water and so for a given calcium nitrate mass. Figure 10 represents this difference as a function of molar number of Ca^{2+}. From the slope of the line (24,661), we can determine the precipitation molar enthalpy of $CaSO_4$, as − 24.6 ± 0.9 kJ per calcium mol or − 247 ± 9 kJ per Fap mol. This value differs from the mean value deduced from iteration (227.3 kJ per Fap mol) by 8%.

The difference between these values could result from the presence of phosphoric acid generated during

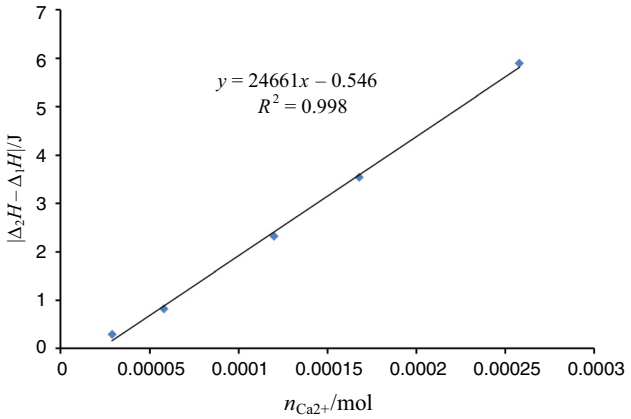

Fig. 10 $|\Delta_2 H - \Delta_1 H|$ as a function of Ca^{2+} molar number

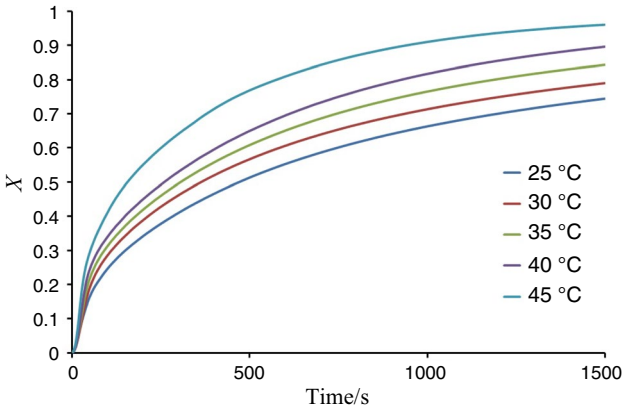

Fig. 11 Variation of the conversion fraction versus time at different temperatures

the attack process while experimental determination of $CaSO_4$ precipitation enthalpy was undertaken without H_3PO_4. This acid could not be added to the precipitation medium otherwise precipitation of calcium sulfate dihydrate ($CaSO_4{\cdot}2H_2O$) occurs, as was shown previously [10].

Attack of the fluorapatite at different temperatures

Thermochemical study

The behavior of the Fap toward the sulfuric acid solution was investigated in 30–45 °C interval by dissolving the same Fap masses (around 36 mg) in 4.5 mL of the acid solution.

The kinetic factors were maintained constant as the concentration of the sulfuric acid solution, the agitation and the solid/liquid ratio.

Experiments performed in the range 30–45 °C show only one peak in the thermogenesis as at 25 °C for masses lower than 40 mg. Solids isolated after each attack at each temperature were characterized by X-ray diffraction and infrared spectroscopy confirming the presence only of anhydrous calcium sulfate as at 25 °C.

The obtained results allow plotting the conversion fraction (X) versus time in Fig. 11, where $X = Q_t/Q_{tot}$, Q_t is the amount of heat at time t and Q_{tot} is the overall amount of heat determined by integrating the whole peak. These curves show an increase in the attack rate at a certain time when the temperature increases, this tendency was expected.

Figure 12 shows the resulting molar enthalpy as a function of temperature. This variation seems to follow the Kirchhoff low: $\Delta_r H_{mes}\ (T) = \Delta_r H^{o}_{mes}(T_o) + \Delta_r C_p\ (T - T_o)$ with $T_0 = 25\ °C$, assuming the heat capacity is constant in the temperature range of 25–45 °C. Figure 12 enables to calculate the reaction heat capacity $\Delta_r C_p$ as 3.782 kJ mol^{-1} K^{-1} by considering the slope of the curve.

Increasing temperature in the 25–45 °C interval leads to a monotonic variation in the reaction molar enthalpy. Same tendency was observed by Zendah et al. [23, 32] for carbonate fluorapatite and Brahim et al. [9, 33] for synthetic fluorapatite dissolution in the hydrochloric acid solution. This result was different from that found by Antar et al. [34] when dissolving Fap in a mixture of phosphoric and sulfuric acid solution.

Kinetic study

For temperature higher than 25 °C, the application of the kinetic model of two successive steps developed above at 25 °C (iteration of Eq. (10)) does not lead to coincidence between the calculated curves and the thermogenesis. So, we applied other models for the heterogeneous reaction.

Shrinking core model (SCM) The well knowing SCM model is used in the heterogeneous solid–fluid reaction. According

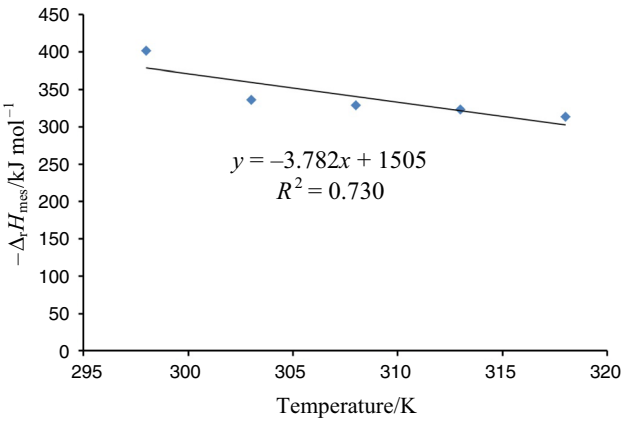

Fig. 12 Kirchhoff representation of the molar dissolution enthalpy versus temperature

to this model, the reaction between a solid and a fluid can be described as:

A (solid) + B (fluid) products (fluid and solid)

The reaction is considered to take place first on the outer surface of the un-reacted particle. During the increase in conversion, the un-reacted core of the particle shrinks and the layer of the resulting solid product thickens.

The following five steps describe the process of the SCM model during reaction [35–37]

(a) Diffusion of a fluid reactant through a fluid film on a solid product
(b) Diffusion of a fluid reactant through a solid product on the surface of a solid reactant
(c) Reaction between a fluid reactant and a solid reactant
(d) Diffusion of a fluid product through a solid product film to a fluid film
(e) Diffusion of a fluid through a fluid film to a bulk fluid.

According to Levenspiel, steps (d) and (e) do not contribute directly to the reaction resistance if no gaseous products are formed. The step with highest resistance is considered to be the rate-controlling step [35–38].

Generally, a heterogeneous reaction is controlled by only diffusion through the fluid film (Eq III), or by the chemical reaction at the surface of the un-reacted solid (Eq IV) or by diffusion through the product layer (Eq V), or by a mixture of diffusion and chemical reaction [35, 39, 40]. Levenspiel [35] proposed for each step the derived integrated rate equations as:

Film diffusion control:

$$X = kt \tag{13}$$

Surface chemical reaction control:

$$[1-(1-X)^{\frac{1}{3}}] = kt \tag{14}$$

Product layer diffusion control:

$$[1-3(1-X)^{\frac{2}{3}}+2(1-X)] = kt \tag{15}$$

In order to determine the rate-controlling step and the effect of temperature on the sulfuric acid attack of Fap, the experimental data were analyzed considering Eqs. (13), (14) and (15) but the results in each case have given no correlation between the experimental data and the theoretical equation with the correlation coefficient (R^2) low than 0.3.

However, it was found that the dominant process of the sulfuric acid attack of the Fap can be a mixture of both diffusion through the ash or product layer and chemical reactions.

Indeed, as shown in Figs. 13 and 14, there is a good correlation between the experimental data and Eq (V) for $t \leq 500$ s and Eq (IV) for $t \geq 500$ s, respectively.

From the slopes of curves of Figs. 13 and 14, k_1 and k_2 constants were calculated and then plotted against $1/T$ in Figs. 15 and 16, respectively. The apparent activation

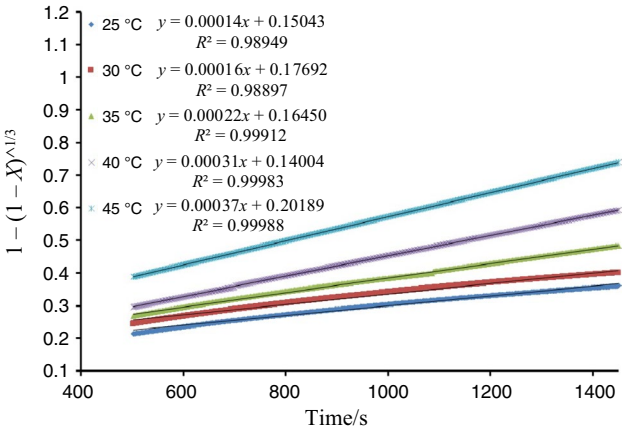

Fig. 14 Plot of Eq. (14) versus time at various temperatures

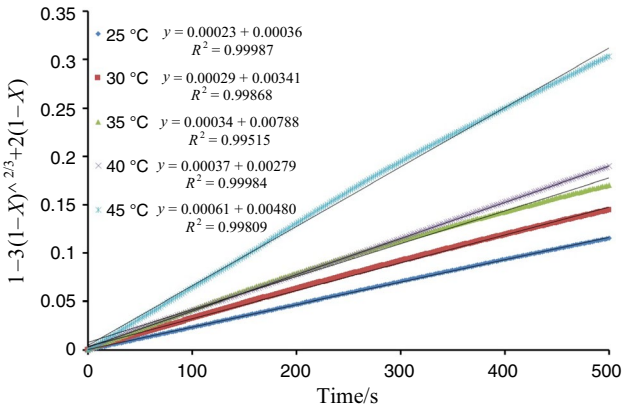

Fig. 13 Plot of Eq. (15) versus time at various temperatures

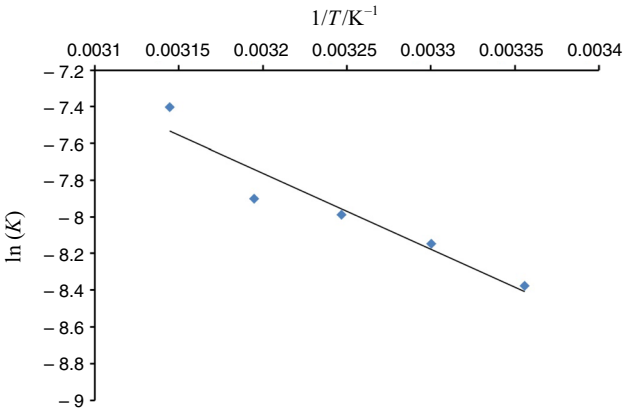

Fig. 15 The plot of ln(k1) (deduced from Fig. 13) against $1/T$

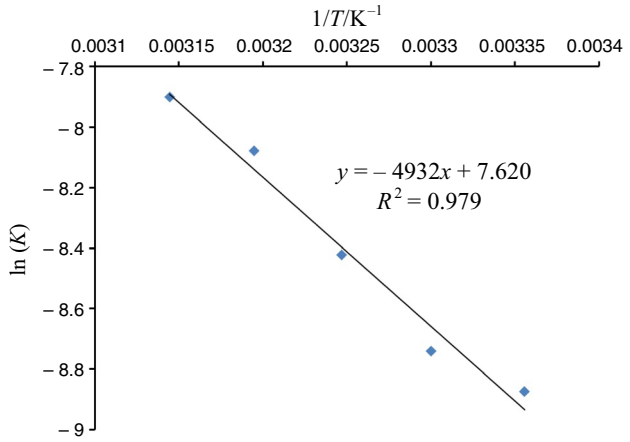

Fig. 16 The plot of ln(k2) (deduced from Fig. 14) against $1/T$

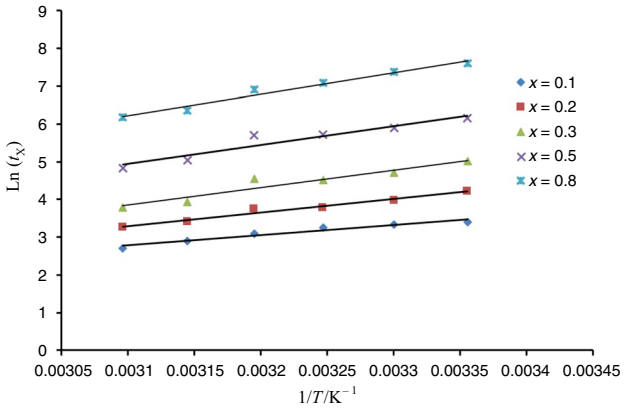

Fig. 17 Examples of plots of Ln(t_x) versus $1/T$ for $25 \le T \le 45$ °C at different x

energies (E_a) were determined as $E_{a1} = 34.4$ kJ mol^{-1} and $E_{a2} = 41.0$ kJ mol^{-1}.

The low value of E_{a1} ($E_{a1} < 40$ kJ mol^{-1}) suggested a diffusion-controlled process. This result agrees with the Avrami one for $n = 0.5$. The latter value has been attributed to a diffusion-controlled growth. The value of the second activation energy E_{a2} is higher than 40 kJ mol^{-1}, in fact it has been reported that the surface chemical reaction-controlling process has activation energy higher than 40 kJ mol^{-1} [35, 40–43]. In our case, the controlled chemical reaction is the contact of C_a^{2+} and SO_4^{2-} ions to form $CaSO_4$.

Isoconversional model In heterogeneous kinetic, the conversion fraction (x) is expressed versus time by the following equation:

$$\frac{dX}{dt} = kf(X) \tag{16}$$

where k is the rate constant and $f(x)$ a function depending on the reaction mechanism.

Integration of Eq (16) leads to

$$g(X) = \int_0^X \frac{dX}{f(X)} = kt \tag{17}$$

Taking into account the Arrhenius law Eq (17) can be arranged as:

$$\ln(t) = \frac{E_a}{RT} + \ln\left(\frac{g(X)}{A}\right) \tag{18}$$

At a certain mole fraction, Ln ($g(X)/A$) is constant [44], and so, it is possible to determine the activation energy, whatever the model, by plotting Ln(t) versus $1/T$.

Figure 17 gives examples of plots at temperature in the range of 25–45 °C for different conversion fractions ($0.05 \le x \le 0.85$).

For one step process, the activation energy is constant along all the process, but in the present case, the experimental data show an increase of E_a on x (Fig. 18). Suggesting that two reaction occur in several steps [44–46], with values of activation energies between 16.7 and 48.8 kJ mol^{-1}. This confirms the appellation "apparent activation energy" in the last section.

It is possible that the reaction is initiated by the Fap dissolution in the sulfuric acid to produce calcium ions which quickly reacts with the acid to form anhydrate calcium sulfate ($CaSO_4$).

Activation energies determined by the SCM models ($E_{a1} = 34.4$ and $E_{a2} = 41.0$) are in the range of values determined by the isoconversional model ($16.7 \le E_a \le 48.8$ kJ mol^{-1}).

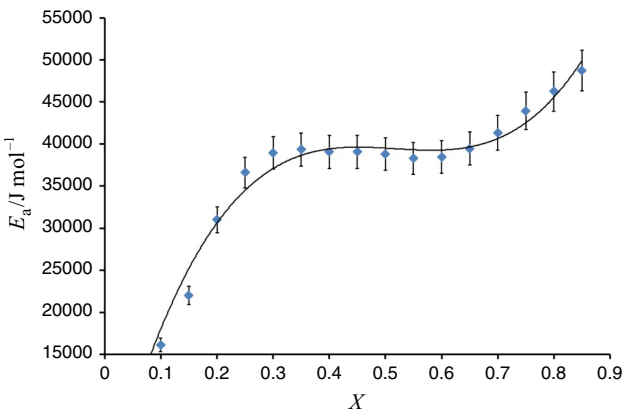

Fig. 18 Dependence of the activation energy versus the conversion fraction according to the isoconversional model

Conclusions

Dissolving a few amount of fluorapatite in 10 mass% H_2SO_4 solution at 25 °C led to the precipitation of anhydrous calcium sulfate ($CaSO_4$). A kinetic mechanism based on successive reactions has been proposed and confirmed thermochemically by comparing the sum of enthalpies deduced from iteration with that obtained by integrating the rough signal. Moreover, the precipitation enthalpy of anhydrous calcium sulfate determined experimentally (-247 ± 9 kJ per Fap mol) differs from the mean value deduced from iteration (227.3 kJ per Fap mol) by 8%. Kinetics of the transformation depends upon the temperature, and the dominant step of the sulfuric acid attack of the Fap is in agreement with a mixture of both diffusion through the ash or product layer and chemical reactions. Isoconversional model confirms the complexity of the process and gives values of activation energies in the range 16.7–48.8 kJ mol^{-1}.

References

1. Dorozhkin SV. A review on the dissolution models of calcium apatites. Prog Cryst Growth Charact Mater. 2002;44:45–61.
2. Harouiya N, Chairat C, Köhler SJ, Gout R, Oelhers EH. The dissolution kinetic and apparent solubility of natural apatite in closed reactors at temperatures from 5 to 50 °C and pH from 1 to 6. Chem Geol. 2007;244:554–68.
3. Gioia F, Mura G, Viola A. Analysis, simulation and optimization of hemihydrate process for the production of phosphoric acid from calcareous phosphites. Ind Eng Chem Process Des Dev. 1977;16(3):390–9.
4. Ashraf M, Zafar ZI, Ansari TM, Ahmed F. Selective leaching kinetics of calcareous phosphate rock in phosphoric acid. J Appl Sci. 2005;5:1722–7.
5. Soussi-Baatout A, Ibrahim K, Khattech I, Jemal M. Attack of Tunisian phosphate ore by phosphoric acid: kinetic study by means of differential reaction calorimetry. J Therm Anal Calorim. 2016;124:1671–8.
6. Sevim F, Sarac H, Kocakerim MM, Yartasi A. Dissolution kinetics of phosphate ore in H_2SO_4 solutions. Ind Eng Chem Res. 2003;42:2052–7.
7. Belgacem B, Leveneur S, Chlendi M, Estel L, Bagane M. The aid of calorimetry for kinetic and thermal study. J Therm Anal Calorim. 2019. https://doi.org/10.1007/s10973-018-7157-3.23456789.
8. Jemal M, Ben Cherifa A, Khattech I, Natahomvukiye I. Standard enthalpies of formation and mixing of hydroxy-, and fluorapatites. J Thermochim Acta. 1995;259:13–21.
9. Brahim K, Khattech I, Dubes JP, Jemal M. Etude cinétique et thermodynamique de la dissolution de la fluorapatites dans l'acide phosphorique à 25°C. Thermochim Acta. 2005;436:43–50.
10. Antar K, Brahim K, Jemal M. Etude cinétique et thermodynamique de l'attaque d'une fluorapatite par des mélanges d'acides sulfurique et phosphorique à 25°C. Thermochim Acta. 2006;449:35–41.
11. Heughebaert JC. Contribution à l'étude de l'évolution des orthophosphates de calcium précipités amorphes en orthophosphates apatitiques. Ph.D. thesis, Institut national polytechnique de Toulouse, Toulouse; 1977.
12. Prener JS. Nonstoichiometry in calcium chlorapatite. J Solid State Chem. 1971;3:49–55.
13. Sands DE. Weighting factors in least squares. J Chem Educ. 1974;51:473–4.
14. Pattengill MD, Sands DE. Statistical significance of linear last squares parameters. J Chem Educ. 1979;56:244–7.
15. Avrami M. Granulation, phase change, and microstructure kinetics of phase change III. J Chem Phys. 1941;9:177–84.
16. Liu M, Zhao Q, Wang Y, Zhang C, Mo Z, Cao S. Melting behaviors, isothermal and non-isothermal crystallization kinetics of nylon 1212. Polymer. 2003;44:2537–45.
17. Yavuz M, Maeda H, Vance L, Liu HK, Dou SX. Phase development and kinetics of high temperature Bi-2223 phase. J Alloys Compd. 1998;281:280–9.
18. Perlovich GL, Bauer-Brandl A. The melting process of acetylsalicylic acid single crystals. J Therm Anal Calorim. 2001;63:653–61.
19. Kabai J. Determination of specific activation energies of metal oxides and metal oxide hydrates by measurement of the rate of dissolution. Acta Chim Acad Sci Hung. 1973;78:57–73.
20. Vaimakis TC, Economou ED, Trapalis CC. Calorimetric study of dissolution kinetics of phosphorite in diluted acetic acid. J Therm Anal Calorim. 2008;92(3):783–9.
21. Fertani-Gmati M, Jemal M. Thermochemistry and kinetics of silica dissolution in NaOH aqueous solution. Thermochim Acta. 2001;513:43–8.
22. Okur H, Tekin T, Ozer AK, Bayramoglu M. Effect of ultrasound on the dissolution of colemanite in H_2SO_4. Hydrometallurgy. 2002;67:79–86.
23. Zendah H, Khattech I, Jemal M. Thermochemical and kinetic studies of the acid attack of "B" type carbonate fluorapatites at different temperatures (25–55)°C. Thermochim Acta. 2013;565:46–51.
24. Papon P, Leblond J, Meijer PHE. The physics of phase transitions concepts and applications. 2nd ed. Berlin: Springer; 2006.
25. Hubert S. Transition de phases solides induites par un procédé de compression directe: Application à la cféine et à la carbamazépine. Ph.D. thesis, University of Lyon; 2012.
26. Kuga N, Sêstak J. Thermoanalytical kinetics and physico-geometry of the nonisothermal crystallization of glasses. Bol Soc Esp Ceram Vidr. 1992;31:185–90.
27. Fosting ER. Phase transformation kinetics and microstructure of carbide and diboride based ceramics. Ph.D. thesis, Fakultät für Bergbau, Hüttenwesen und Maschinenwesen of the Technische Universität Clausthal; 2005.
28. Brahmia N. Contribution à la modélisation de la cristallisation des polymères sous cisaillement: application à l'injection des polymères semi-cristallins.Ph. D. thesis, Institut National des Sciences Appliquées de Lyon; 2007.
29. Rao CNR, Rao KJ. Phase transitions in solids, an approach to the study of the chemistry and physics of solids. New York: McGraw-Hill Inc; 1978.
30. Antar K, Jemal M. Kinetics and thermodynamics of the attack of fluorapatite by a mixture of sulfuric and phosphoric acids at 55°C. Thermochim Acta. 2007;452(1):71–5.
31. Mandal PK, Mandal TK. Anion water in gypsum ($CaSO_4 \cdot 2H_2O$) and hemihydrate ($CaSO_4 \cdot 1/2H_2O$). Cem Concr Res. 2002;32:313–6.
32. Zendah H, Contribution à l'étude thermochimique et cinétique de l'attaque par l'acide phosphorique de fluorapatites synthétiques variablement carbonatées, Ph.D. thesis, Université de Tunis El Manar, Tunis; 2013.
33. Brahim K. Contribution à l'étude thermodynamique et cinétique de l'attaque phosphorique d'une fluorapatite: Application à un

phosphate naturel, Ph.D. thesis, Université de Tunis El Manar, Tunis; 2006.
34. Antar K, Jemal M. Kinetics and thermodynamics of the attack of a phosphate ore by acid solutions at different temperatures. Thermochim Acta. 2008;474:32–5.
35. Levenspiel O. Chemical reaction engineering. 3rd ed. New York: Wiley; 1999.
36. Sohn H, Wadsworth ME. Rate processes of extractive metallurgy. New York: Plenum Press; 1979.
37. Habashi F. Principles of extractive metallurgy. New York: Gordon and Breach; 1979.
38. Tekin G, Onganer Y, Alkan M. Dissolution kinetics of ulexite in ammonium chloride solution. Can Metall Q Can J Metall Mater Sci. 2013;37(2):91–7.
39. Gharabaghi M, Irannajad M, Noaparast M. A review of the beneficiation of calcareous phosphate ores using organic acid leaching. Hydrometallurgy. 2010;103(1–4):96–107.
40. Zafar ZI. Determination of semi empirical kinetic model for dissolution of bauxite ore with sulfuric acid: parametric cumulative effect on the Arrhenius parameters. J Chem Eng. 2008;141:233–41.
41. Souza AD, Pina PS, Leâo VA, Silva CA, Siqueira PF. The leaching kinetics of a zinc sulphide concentrate in acid ferric sulphate. Hydrometallurgy. 2007;89:72–81.
42. Abdel-Aal EA, Rashed MM. Kinetic study on the leaching of spent nickel oxide catalyst with sulfuric acid. Hydrometallurgy. 2004;74:189–94.
43. Calmanovici CE, Gilot B, Laguérie C. Mechanism and kinetics for the dissolution of apatitic materials in acid solutions. Braz J Chem Eng. 1997;14(2):95–102.
44. Sbirrazzuoli N, Brunel D, Elegant L. Different kinetic equations analysis. J Therm Anal Calorim. 1992;38:1509–24.
45. Vyazovkin S. Evaluation of activation energy of thermally stimulated solid-state reactions under arbitrary variation of temperature. J Comput Chem. 1997;18:393–402.
46. Fertani-Gmati M, Jemal M. Thermochemical and kinetic investigations of amorphous silica dissolution in NaOH solutions. J Therm Anal Calorim. 2016;123:757–65.